Brodogradnja/Shipbilding Volume 66 Number 1, 2015

Lamas, M.I.
Rodríguez, C.G.
Rodríguez, J.D.
Telmo, J.

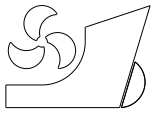

ISSN 0007-215X
eISSN 1845-5859

NUMERICAL ANALYSIS OF SEVERAL PORT CONFIGURATIONS IN THE FAIRBANKS-MORSE 38D8-1/8 OPPOSED PISTON MARINE ENGINE

UDC 629.5.026:621.43.011:621.436
Original scientific paper

Summary

The aim of the present paper is to analyze several port configurations in the Fairbanks-Morse 38D8-1/8 marine diesel engine. The motivation comes from the high number of intake and exhaust ports which characterizes this engine. The scavenging and trapping efficiency were studied by modifying several parameters related to the ports, such as the inclination, shape, pressure and number. To this end, a numerical model based on the commercial software ANSYS Fluent was employed. Numerical results were validated using experimental measurements performed on a Fairbanks-Morse 38D8-1/8 engine installed on a submarine. The results confirmed that the influence of the port shape is practically negligible; nevertheless, an adequate combination of the inclination, pressure and number of ports can modify the scavenging and trapping efficiency noticeably.

Key words: *diesel engine; scavenging; CFD (Computational Fluid Dynamics).*

1. Introduction

An opposed-piston engine is an internal combustion engine in which each cylinder has a piston at both ends, and no cylinder head. These engines were employed from the end of the nineteen century with the intention of improving the performance of two-stroke diesel engines. One of its advantages is the use of uniflow scavenging, much more efficient than loop or cross scavenging. Another advantages of opposed-piston engines are that unsymmetrical port timing improves the efficiency and performance by optimizing the timings (the exhaust opening point can be advanced and the inlet closing point can be delayed), lower piston speeds because the stroke is split into two pistons, no cylinder heads (avoiding the problem of heat losses to the jacket water), no valve mechanisms (avoiding their cooling and lubricating problems), fewer moving parts, etc.

In the field of opposed-piston engines, the Fairbanks-Morse Model 38D8-1/8 is a medium-speed, two-stroke diesel engine with a design inspired on German Junkers engines.

It has consolidated its success though many decades of manufacturing and thousands of units sold for marine propulsion, electric power plants and numerous mechanical drive applications. Although it was firstly developed in the 1930s for locomotive use, it was mostly used to propel submarines in World War II. Tambor class, Gato class, Balao class, Tench class, or more recently, Tang class, are submarines propelled by this engine. Its success in submarine service made Fairbanks-Morse a strong contender for post-war diesel marine engine sales. Its commercial production began in 1938 for several uses. Concerning ship propulsion, it was employed in many civilian ships such as tugs, fishing and small vessels in general. Nowadays, more than 80 years since the first prototypes, Fairbanks-Morse opposed-piston engines are still in production, mainly in the field of marine propulsion.

When improving the efficiency of these engines, there are too involving variables. Although nowadays there are many experimental techniques, Computational Fluid Dynamics (CFD) offers an alternative method to study the fluid flow inside the cylinder. In the field of medium and large engines, CFD is especially useful because experimental setups are extremely expensive and laborious, and down-scale models sometimes are not accurate enough. Nevertheless, their CFD simulation is complicated due to the big size, which requires high computational resources. Since the nineties, advancements in computer hardware have facilitated simulations of big geometries. Nevertheless, only a few works about medium and large engines can be found in the literature. One can refer to the following authors. Nakagaya *et al*. [1] developed a bidimensional CFD model to study a large two-stroke diesel engine. Andersen *et al.* [2, 3] cantered on the scavenging process of marine engines. Bigos and Puskar [4] analyzed the influence of the cylinder shape and combustion space. Sigurdsson [5, 6] examined the scavenging process of the MAN B&W 4T50MX test engine. Haider [7] developed a numerical and experimental study of the swirling flow during part of the scavenging process of a downscale model of the MAN B&W 4T50MX test engine. Lamas and Rodríguez [8] studied the scavenging process in the MAN 7S50MC and the effect of EGR and water addition during the combustion process, Lamas *et al*. [9]. They also analyzed the valve overlap period in the Wärtsilä 6L 46 [10], the combustion process [11], and internal modifications to reduce pollutant emissions [12]. Larbi and Bessrour [13] analyzed numerically the emissions of the Wärtsilä 6R32 and the effect of EGR [14], ammonia injection [15] and water injection [16]. Kontoulis *et al.* [17] analyzed the combustion and emissions in a large two-stroke marine diesel engine. Kilpinen [18] focused on NO emission in 4-stroke marine engines. Seddiek and Elgohary [19] centered on an analysis of SO_x and NO_x emissions.

The aim of the present paper is to develop a CFD model to optimize the scavenging process of opposed-piston engines, *i.e.*, the action of displacing the burnt gases from the cylinder and replacing them by the fresh-air charge. Particularly, the Fairbanks-Morse 38D8-1/8 marine engine was studied. The scavenging and trapping efficiency were analyzed in terms of several port configurations. Previously to this, numerical results were successfully compared with experimental measurements performed on a Fairbanks-Morse 38D8-1/8 engine installed on a submarine.

2. Materials and methods

2.1 Case studied

For the present work, a 38D8-1/8 installed on a submarine, Fig. 1, was employed. This engine has 8 cylinders and consequently 16 pistons. Each cylinder has 16 inlet ports and 10 exhaust ports.

Fig. 1 Fairbanks-Morse 38D8-1/8 installed on a submarine

Figure 2 outlines the geometry. As can be seen, there are two pistons per cylinder and no cylinder head. The combustion space is formed in the center of the cylinder between both pistons, which move away from each other. The exhaust ports are located near the bottom of the cylinder and the inlet ports near the top. The ports are controlled by the movement of the pistons as they reach the outer positions of their travel, thus eliminating the use of valves. When the ports are covered/uncovered by a piston, they are closed/opened respectively. The pistons controlling the air-inlet ports are located in the upper crankshaft, while those controlling the exhaust ports are located in the lower crankshaft. Both crankshafts are connected together by a vertical drive gearing. The crankshafts turn in opposite directions and the upper crankshaft has a 12-degree angle delay over the lower crankshaft, permitting asymmetrical port timing. There are two fuel injection nozzles per cylinder, directly across from each other on the liner wall, that inject fuel into a firing chamber formed by the heads of the two pistons. For marine service, the engine is built directly reversible. Naturally, port timing is not optimum during reverse operation.

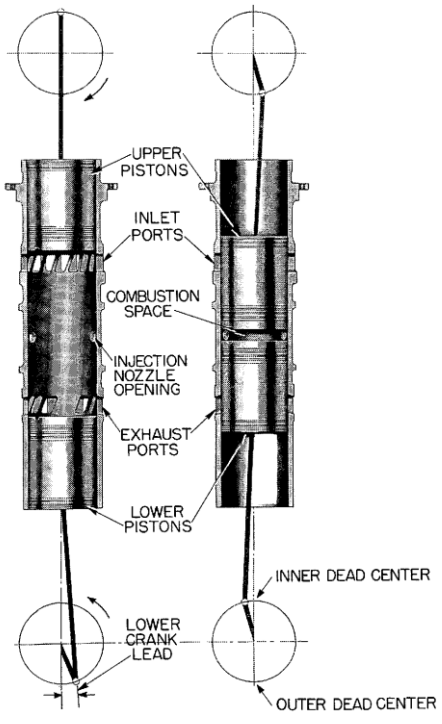

Fig. 2 Cylinder geometry, Fairbanks-Morse & Co [20]

The cycle of operation begins with the movement of the pistons from their outer dead centres. Fig. 2 (a) shows the lower crankshaft past outer dead centre and the upper crankshaft at outer dead centre. At this moment, the inlet and exhaust ports are opened (uncovered by the pistons), and consequently fresh air supplied by a blower is being admitted into the cylinder and exhaust gases are being expelled. As the pistons move inward, they close (cover) the exhaust and inlet ports and the air inside the cylinder is compressed. As mentioned above, the combustion space is formed between recessed heads of the two pistons as the crankshafts approach inner dead centre, Fig. 2 (b). At approximately 9º before the lower piston reaches inner dead centre, the injection of fuel oil begins. The high temperature and pressure of the air charge causes the fuel oil to ignite and combustion takes place. The high pressures resulting from combustion force the pistons to move outward, delivering power to the crankshafts. The expanding of the gases continues until the lower piston begins to open (uncover) the exhaust ports, allowing the burnt gases to escape to the atmosphere through the exhaust system. After that, the upper piston opens (uncovers) the inlet ports and scavenging air rushes into the cylinder. Finally, the cylinder is swept clean of the remaining exhaust gases and refilled with fresh air for the next compression stroke.

2.2 Numerical implementation

The engine described in the previous section was studied numerically. Particularly, the scavenging process was studied along a period of time from 90º lower crankshaft angle to 270º lower crankshaft angle.

Concerning the governing equations, the turbulent flow is governed by the conservation of mass, momentum and energy. Besides, one more equation is needed to characterize the local mass fraction of air and burnt gases. Turbulence was simulated by the *k-ε* model because it is robust, economic and reasonably accurate for a wide range of CFD cases.

All CFD models require initial and boundary conditions. Concerning the pressures, their values were measured experimentally. The initial (90º lower crankshaft angle) in-cylinder gauge pressure is 3.2 bar, the exhaust gauge pressure is 0.1 bar and the inlet gauge pressure, given by a lobe rotary compressor, is 0.4 bar. The inlet temperature was also experimentally measured, corresponding to 325 K. The inlet pressure, exhaust pressure and inlet temperature were provided by the engine itself. Nevertheless, the in-cylinder pressure was measured by a pressure sensor Leutert DPI-F2, which provided the PV diagram.

Concerning the heat transfer from the cylinder to the cooling water, a combined convection-radiation type was assumed:

$$q = h(T_{gas} - T_{water}) \tag{1}$$

where q is the heat transferred, T_{gas} the in-cylinder temperature, T_{water} the cooling water temperature, 81.2ºC according to experimental measurements, and h the heat transfer coefficient (due to convection + radiation), given by the following expression, Taylor [21]:

$$h = 10.4kb^{-1/4}(u_{piston}/\nu)^{3/4} \tag{2}$$

where b is the cylinder bore, k the thermal conductivity, u_{piston} the mean piston speed, and ν the kinematic viscosity. Substituting values into the equation above yields h = 3593 W/m^{2}K.

As all cylinders are identical, only one of them was simulated. The CAD 3D design of the cylinder and ports was realized using Solid Edge ST software. Concerning the pistons, they were not modeled because only the surfaces in contact with the fluids are needed for the computations.

The mesh was created by Gambit 2.4 and then exported to ANSYS Fluent 6.3. In order to implement the movement of the pistons, a deforming mesh was used. As it was verified that hexahedral elements provide better accuracy and stability than tetrahedral ones [22], a structured hexahedral mesh was adopted. In order to take into account the boundary layer, a finer mesh was employed near the walls. The mesh motion is shown in Fig. 3, in which the arrows indicate the direction of the pistons. The number of cells varies from 50000 to 350000. Figure 3 (a) represents the start of the simulation, 90º lower crankshaft angle. As can be seen, the ports are uncovered by the piston and thus there is no fluid flow between the cylinder and ports, and the pistons start to move outward. Figure 3 (b) represents the position 200º lower crankshaft angle. At this moment, the ports are covered by the piston and thus there is fluid flow between the cylinder and ports, remaining opened, and the pistons move inward. Finally, Fig. 3 (c) represents the end of the simulation with no fluid flow and the pistons moving inward.

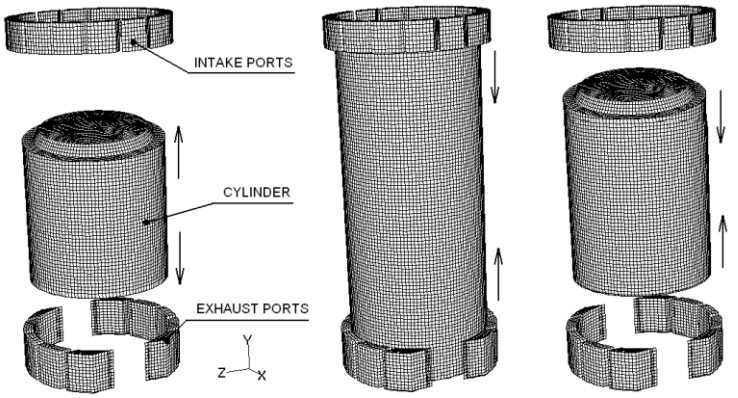

Fig. 3 Mesh motion. (a) 90º lower crankshaft angle; (b) 200º lower crankshaft angle; (c) 270º lower crankshaft angle

ANSYS Fluent is based on the finite volume method. The PISO algorithm was chosen for pressure-velocity coupling. A second order scheme was employed to discretize the continuity, momentum, energy and mass fraction equations. The time derivatives were discretized through a first order fully implicit scheme. Both mesh size and time step were analyzed to ensure that suitable values were employed.

3. Results and discussion

First of all, this section describes the results and validation of the model. After that, the scavenging and trapping efficiency are studied against several port configurations.

3.1 Mass fraction, pressure and velocity fields

Figure 4 shows the mass fraction field of air for several values of the lower crankshaft angle. It was represented the start of the simulation (90º), end of the simulation (270º), outer dead center of the lower crankshaft (180º), outer dead center of the upper crankshaft (192º) and other representative instants. It can be observed that initially the cylinder is full of burnt gases, Fig. 4 (a) and the pistons are moving outward, as indicated by the arrows. There is no any mass fraction passing inside the chamber as all ports are closed (covered by the pistons). After the exhaust ports are opened (uncovered), Fig. 4 (b), the burnt gases begin to flow out. Thereafter, the inlet ports are opened (uncovered) and consequently pressurized air enters the chamber and helps to throw the burnt gases away, Fig. 4 (c-d). After reaching 192º, the pistons move inward. Air continues flowing into the cylinder and burnt gases continue

flowing out, Fig. 4 (e-f). Finally, the inlet ports and then exhaust ports are closed (covered by the pistons), and at the end of the simulation, Fig. 4 (g), the cylinder contains a mixture of air and a small amount of residual gases which were not expelled.

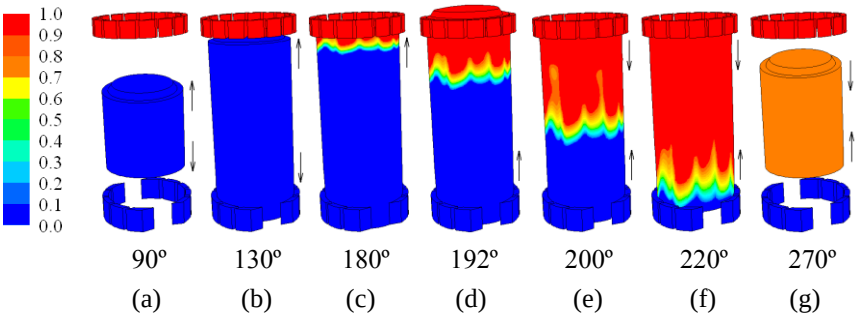

Fig. 4 Mass fraction field of air for several lower crankshaft angles

Figure 5 shows the velocity field. It can be seen that, when the exhaust ports are opened, Fig. 5 (a), burnt gases are expelled. When all ports are opened, Fig. 5 (b), air is admitted into the cylinder through the inlet ports and burnt gases are expelled through the exhaust ports. The pressure difference from the top to the bottom zones of the cylinder causes a motion from the intake to the exhaust ports. As can be seen in Fig. 5 (c), Section A-A, the inlet ports have an inclination of 20.9º around the cylinder axis. This promotes a swirling motion which is vanished as the fluid descends in the direction of the exhaust ports, shown in Section B-B.

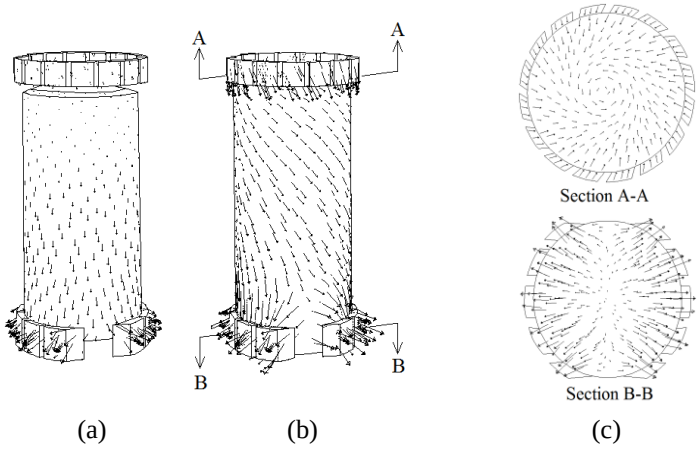

Fig. 5 Velocity field (m/s). (a) 130º lower crankshaft angle; (b) 200º lower crankshaft angle; (c) transversal sections at 200º lower crankshaft angle. → 200 m/s

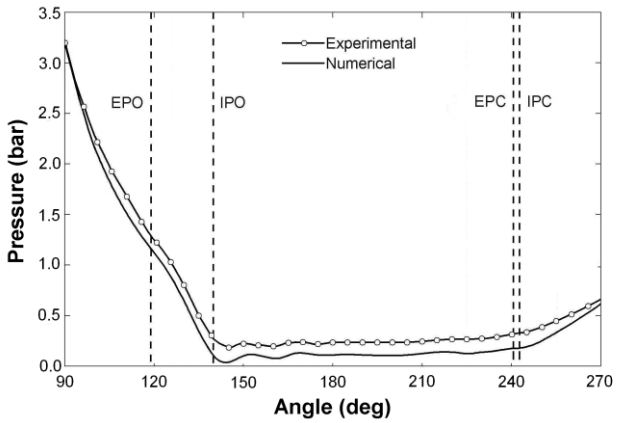

Fig. 6 In-cylinder gauge pressure (bar). EPO: exhaust ports opening; IPO: inlet ports opening; EPC: exhaust ports closing; IPC: inlet ports closing

Figure 6 shows the time history of the in-cylinder average gauge pressure. The calculated pressure was validated with experimental measurements, which also are represented in this figure. A good agreement between numerical and experimental results was obtained, being the average error 5.6%. Many factors are responsible for the difference between numerical and experimental results. CFD itself implies an error in the mesh generation and discretization process. The hypotheses assumed to simplify the computations constitute another source of errors.

3.2 Analysis of the scavenging and trapping efficiency

The scavenging efficiency indicates to what extent the burnt residuals have been replaced with fresh charge. It is computed as the mass of delivered air that was trapped by comparison with the total mass of charge that was retained at exhaust closure, Eq. (3). The present CFD simulation provided a value of 86.2% for the parameters studied. This value satisfactory agrees with the 90% indicated elsewhere for this engine, Schweitzer [23].

$$SE(\%) = 100\,\frac{\text{mass of delivered air retained}}{\text{mass of mixture in the cylinder}} \tag{3}$$

On the other hand, the trapping efficiency indicates, from the air mass inducted in the cylinder, the fraction really retained. The CFD simulation provided 77.6% for the conditions studied.

$$TE(\%) = 100\,\frac{\text{mass of delivered air retained}}{\text{mass of delivered air}} \tag{4}$$

It is interesting to analyze the effect of some parameters on the scavenging and trapping efficiency. The first parameter studied was the intake ports inclination, employed in engines with uniflow scavenging in order to improve the scavenging process. The inclination induces a swirling flow which minimizes the amount of residual gases that remain trapped without being expelled.

As stayed above, the intake ports are inclined 20.9º. The results of scavenging and trapping efficiency for other values are represented in Fig. 7. As can be seen, as the inclination is increased the scavenging efficiency increases and then decreases. The reason is that the intake ports inclination optimizes the orientation of the flow inside the cylinder. Nevertheless, an excessive swirl promotes an inadequate movement which reduces the scavenging efficiency. For the same reason, the trapping efficiency also increases and then decreases with the inclination of the intake ports.

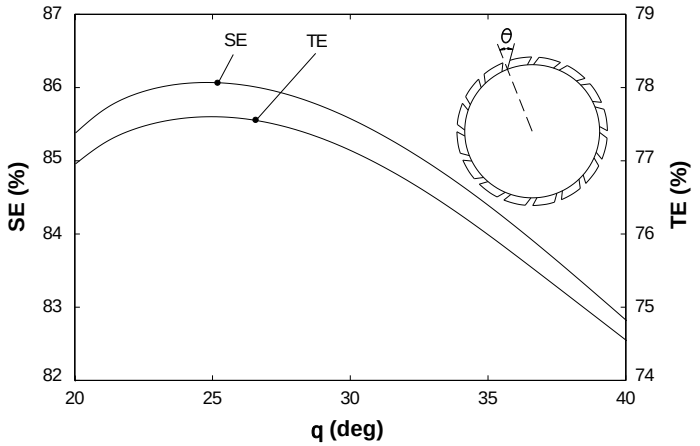

Fig. 7 Scavenging and trapping efficiency against the intake ports inclination

Another interesting parameter is the intake pressure given by the compressor. For this engine, the intake pressure is 0.4 bar. Fig. 8 shows the scavenging and trapping efficiency for other values of the intake pressure. As can be seen, the scavenging efficiency increases with pressure. The reason is that high pressures promote a more intense entrance of air from the inlet to the exhaust and consequently a higher amount of air is retained inside the cylinder. On the contrary, the trapping efficiency decreases with the inlet pressure because the amount of delivered air is highly increased with the intake pressure. High inlet pressures promote a high quantity of delivered air and, consequently, a lower trapping efficiency.

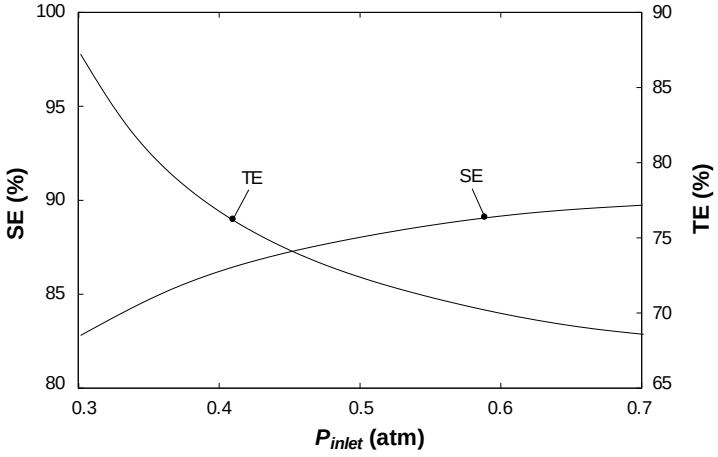

Fig. 8 Scavenging and trapping efficiency against the inlet pressure

Another aspect is the port shape. For the purpose three shapes were studied, rectangular, circular and elliptical, Fig. 9. At equal areas, the scavenging and trapping efficiency against the intake and exhaust ports shape are indicated in Table 1. As can be seen, the effect of the shape is almost negligible. The circular port has low drag losses due to its low relation perimeter/area. The most similar port is the elliptical, followed by the rectangular. For this reason, the scavenging efficiency is higher for the circular intake port shape, followed by the elliptical and rectangular. The low drag of the circular shape allows air to enter the cylinder easily and consequently increases the amount of air which remains trapped. On the contrary, the trapping efficiency is lowest for the circular intake port shape, followed by the elliptical and rectangular. The reason is that a higher amount of entering air implies a reduction of the trapping efficiency. Concerning the exhaust ports shape, the scavenging and trapping efficiency are highest for the circular shape, followed by the elliptical and rectangular ones.

The reason is that the amount of air retained in the cylinder is higher as the drag at the exhaust ports increases.

Table 1 Efficiency against the shape of the ports

		Rectangular	Circular	Elliptical
Intake ports	SE (%)	86.2	86.5	86.4
	TE (%)	77.6	77.3	77.4
Exhaust ports	SE (%)	86.2	85.9	86.0
	TE (%)	77.6	77.4	77.5

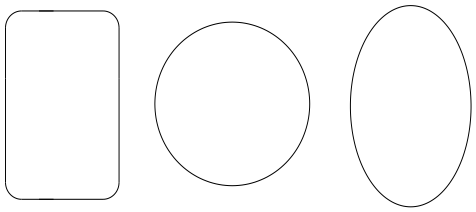

(a) (b) (c)

Fig. 9 Exhaust port configurations. (a) rectangular; (b) circular; (c) elliptical

Finally, the last parameter studied is the number of ports. At equal total area, Figs. 10 and 11 show the scavenging efficiency and trapping efficiency against the number of intake and exhaust ports respectively. As can be seen, the scavenging and trapping efficiency increase with the number of both intake and exhaust ports. The reason is that the fluid is better directioned as the number of ports is increased. It is important to note that the number of the intake ports is more important than the number of the exhaust ports because the former is related to the swirl movement necessary to scavenge. Nevertheless, the exhaust ports have a low influence in the swirl movement. The trapping and scavenge efficiency decreases with the number of exhaust ports because it is easier the emerging of flow from the cylinder.

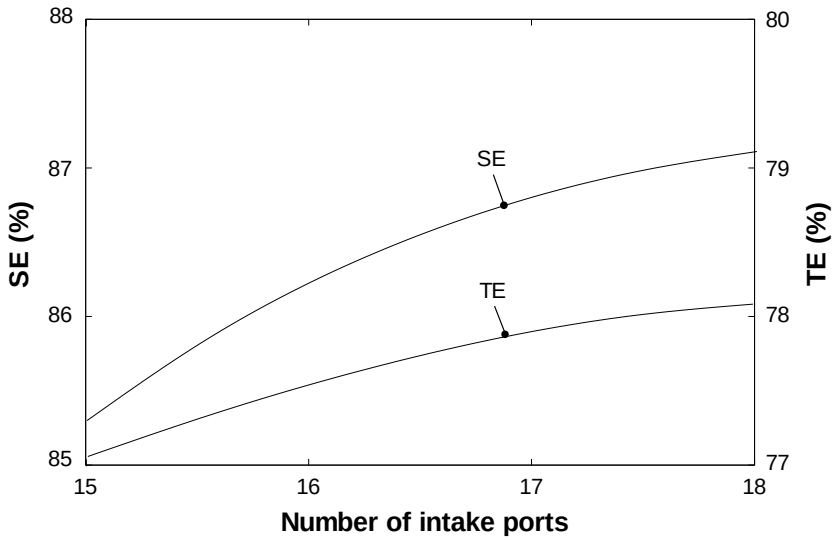

Fig. 10 Scavenging and trapping efficiency against the number of intake ports

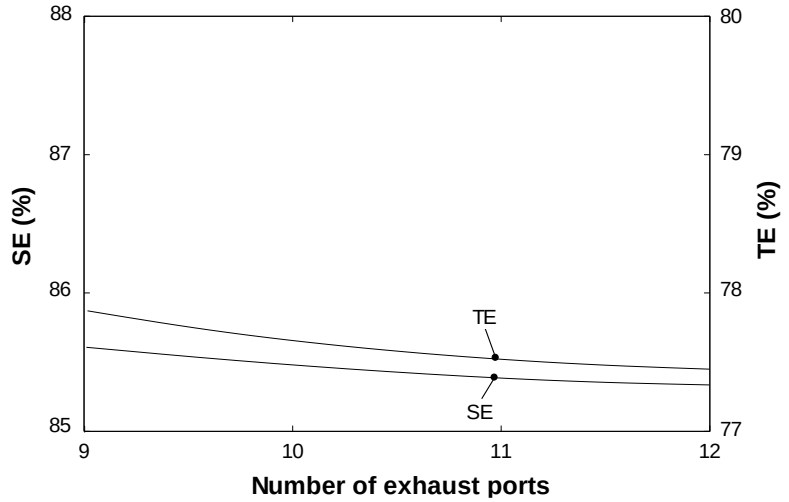

Fig. 11 Scavenging and trapping efficiency against the number of exhaust ports

4. Conclusions

In the present work, a CFD analysis was developed to study the scavenging process of the Fairbanks-Morse 38D8-1/8 opposed-piston marine diesel engine. The results were satisfactory compared with experimental measurements carried out in an engine installed on a submarine. In general, this study shows that CFD predictions yield reasonably accurate results that can help to improve the knowledge of the flow characteristics at the scavenging process. Particularly, an error of 5.6% was obtained in the in-cylinder average pressure.

Once validated, this numerical model was employed to study the scavenging efficiency in terms of several modifications of the exhaust and intake ports. It was verified that the influence of the port shape is practically negligible. Nevertheless, the inclination, pressure and number of ports can modify the scavenge and trapping efficiency noticeably.

5. Acknowledgements

The authors would like to express their gratitude to “Talleres Pineiro, S.L.”, sale and repair of marine engines.

REFERENCES

[1] Nakagawa, H.; Kato, S.; Tateishi, M.; Adachi, T.; Tsujimura, H.; Nakashima, M.: Airflow in the cylinder of a 2-stroke cycle uniflow scavenging diesel engine during compression stroke, JSME International Journal Series II, Vol. 33, p. 591-598, 1990.

[2] Andersen, F.H.; Hult, J.; Nogenmyr, K.J.; Mayer, S. Numerical investigation of the scavenging process in marine two-stroke diesel engines. SAE Technical Papers. SAE/KSAE 2013 International Powertrains, Fuels and Lubricants Meeting, FFL 2013; Seoul; South Korea; 21 October 2013 through 23 October 2013; Code 1008742013.

[3] Andersen, F.G.; Hult, J.; Nogenmyr, K.J.; Mayer, S.: CFD analysis of the scavenging process in marine two-stroke diesel engines. ASME 2014 Internal Combustion Engine Division Fall Technical Conference, ICEF 2014; Columbus; United States; 19 October 2014 through 22 October 2014; Code 109560.

[4] Bigos, P.; Puskar, M.: Influence of cylinder shape and combustion space on engine output characteristic of two-stroke combustion engine, Zdvihací zařízení v teorii a praxi, Vol. 3, 2008.

[5] Sigurdsson, E.: Scavenging flow in a two-stroke diesel engine. Master Thesis, Technical University of Denmark, 2011.

[6] Sigurdsson, E., Ingvorsen, K.M., Jensen, M.V., Mayer, S., Matlok, S., Walther, J.H. Numerical analysis of the scavenge flow and convective heat transfer in large two-stroke marine diesel engines, Applied Energy, Vol. 123, p. 37-46, 2014.

[7] Haider, S.: Experimental and numerical study of swirling flow in scavenging process for 2-stroke marine diesel engine, Ph. D. Thesis, Technical University of Denmark, 2011.

[8] Lamas, M.I.; Rodriguez, C.G.: Computational fluid dynamics analysis of the scavenging process in the MAN B&W 7S50MC two-stroke marine diesel engine, Journal of Ship Research, Vol. 56, No. 3, p. 154-161, 2012.

[9] Lamas, M.I.; Rodriguez, C.G.; Aas, P.: Computational fluid dynamics analysis of NOx and other pollutants in the MAN B&W 7S50MC marine engine and effect of EGR and water addition, International Journal of Maritime Engineering, Vol. 155, Part A2, p. 81-88, 2013.

[10] Lamas, M.I.; Rodriguez, C.G.; Rebollido, J.M.: Numerical model to study the valve overlap period in the Wärtsilä 6L 46 four-stroke marine engine, Polish Maritime Research, Vol. 19, No. 1(72), p. 31-37, 2012.

[11] Lamas, M.I.; Rodriguez, C.G.: Numerical model to study the combustion process and emissions in the Wärtsilä 6L 46 four-stroke marine engine, Polish Maritime Research, Vol. 20, No. 2(78), p. 61-66, 2013.

[12] Lamas, M.I.; Rodriguez, C.G.; Rodríguez, J.D.; Telmo, J.: Internal modifications to reduce pollutant emissions from marine engines. A numerical approach, International Journal of Naval Architecture and Ocean Engineering, Vol 5 (4), p. 493-501, 2013.

[13] Larbi, N.; Bessrour, J.: Experimental measure and simulation of pollutant emissions from marine diesel engine, Physical and Chemical News, Vol.45, p. 80-90, 2009.

[14] Larbi, N.; Bessrour, J.: Measurement and simulation of pollutant emissions from marine diesel combustion engine and their reduction by exhaust gas recirculation, Journal of Mechanical Science and Technology, Vol. 22, p. 2263-2273, 2008.

[15] Larbi, N.; Bessrour, J.: Measurement and simulation of pollutant emissions from marine diesel combustion engine and their reduction by ammonia injection, Advances in Mechanical Engineering, 459813, 2009.

[16] Larbi, N.; Bessrour, J.: Measurement and simulation of pollutant emissions from marine diesel combustion engine and their reduction by water injection, Advances in Engineering Software, Vol. 41, p. 898-906, 2010.

[17] Kontoulis, P.; Chryssakis, C.; Kaiktsis, L.: Analysis of combustion and emissions in a large two-stroke marine diesel engine, using CFD and T-w mapping, Proceedings, 18th International Multidimensional Engine Modeling User's Group Meeting at the Society of Automotive Engineers Congress, Detroit, MI., 2008.

[18] Kilpinen, P.: Optimization of a simplified sub-model for NO emission prediction by CFD in large 4-stroke marine diesel engines, Fuel Processing Technology, Vol 91 (2), p. 218–228, 2010.

[19] Seddiek, I.S.; Elgohary, M.M.: Eco-friendly selection of ship emissions reduction strategies with emphasis on SOx and NOx emissions, International Journal of Naval Architecture and Ocean Engineering, Vol. 6, No. 3, p. 737-748, 2014.

[20] Fairbanks-Morse & Co.: Fairbanks Morse model 38D8-1/8 diesel marine, Engine service manual, 1967.

[21] Taylor, C.F.: The internal combustion engine in theory and practice, 2nd Edition, MIT Press, 1985.

[22] Lamas-Galdo, M.I.; Rodríguez-Vidal, C.G.; Rodríguez-García, J.D.; Fernández-Quintás, M.V.: Modelo de mecánica de fluidos computacional para el proceso de barrido en un motor Otto de dos tiempos. Dyna (Spain), Vol 86, No. 2, p. 165-172, 2011.

[23] Schweitzer, P.H.: Scavenging of two-stroke diesel engines, The Macmillan Company. New York, 1959.

Submitted: 14.01.2015.
Accepted: 02.03.2105.

Lamas, M.I., isabellamas@udc.es, University of A Coruña
Escuela Politécnica Superior. C/Mendizábal s/n. 15403 Ferrol. A Coruña. Spain
Rodríguez, C.G., c.rodriguez.vidal@udc.es, University of A Coruña
Rodríguez, J.D., jdedios@udc.es, University of A Coruña
Telmo, J., javier.telmo@usc.es, University of Santiago de Compostela